# Chapter 14
# Dynamic Properties by OMA and Modal Updating of a Mayan Temple

**T. Nunez and C. E. Ventura**

**Abstract** This paper presents a study on the dynamic properties of the ancient Mayan Temple of the Masks (Temple II) in Tikal, Guatemala, using Operational Modal Analysis (OMA) and finite element (FE) model updating. Built around 700 A.D., the temple is a key funerary and ceremonial monument whose preservation requires continuous structural monitoring. Field OMA measurements were performed to identify modal frequencies, damping ratios, and mode shapes, establishing a baseline for FE model calibration. A simplified FE model was first tuned using geometric data, dynamic properties, and sclerometric test results that characterized the stone's mechanical strength. A refined model was then updated with field data to estimate the temple's seismic response and evaluate the effects of material degradation on long-term stability. This integrated methodology—combining ambient vibration testing and detailed numerical modelling—provides a robust framework for heritage conservation, highlighting how advanced monitoring and modelling techniques can safeguard culturally significant structures like Temple II.

**Keywords** SHM · Laser Scan · Heritage · Soil-Struct Interaction

## Introduction

### *Significance of the Temple of the Masks in Tikal*

The Temple of the Masks (Temple II) in Tikal, Guatemala, built around 700 A.D., reflects the architectural and ceremonial sophistication of the Classic Maya. Facing Temple I across the Great Plaza, it was likely dedicated to Lady Kalajuun Une' Mo', wife of King Jasaw Chan K'awiil I, and marks a period of cultural renewal. Preserving Temple II is crucial due to its historical significance and exposure to environmental and geotechnical hazards. As noted by Rossi and Bournas [3], safeguarding structural health is key for heritage conservation. Modern SHM techniques—vibration analysis, laser scanning, and material testing—provide essential data on performance and deterioration. The temple's location on unstable soil highlights the importance of soil–structure interaction, which is often overlooked in conservation. Interdisciplinary studies combining structural and geotechnical insights [1],[2] are key to minimizing potential hazards. Furthermore, its astronomical alignments [5] enhance its cultural importance. Integrating vibration monitoring, laser scanning, and computational modelling supports a holistic, sustainable strategy to preserve this emblematic Maya monument.

### *Importance of monitoring structural integrity for archaeological preservation*

Preserving archaeological monuments like Temple II in Tikal is challenging due to limited architectural documentation, scarce data on material degradation, and few records of environmental or seismic impacts. These gaps make conservation efforts more difficult and increase the risk of unnoticed deterioration. SHM offers a quantitative framework to address these issues through tools such as ambient vibration monitoring, 3D laser scanning, drone photogrammetry, and ground-penetrating radar (GPR). Vibration monitoring identifies modal frequencies, damping ratios, and mode shapes—key indicators of structural change [6],[7]—while laser scanning and drones provide high-resolution geometric data for detecting deformations

T. Nunez · C.E. Ventura
The University of British Columbia, Department of Civil Engineering
e-mail: nuneztom@mail.ubc.ca; ventura@civil.ubc.ca

© The Author(s), under exclusive license to River Publishers 2026

Kristin B. Zimmerman, PhD (eds.), *Dynamics of Civil Structures, 2026, Vol. 2*, Conference Proceedings
of the Society for Experimental Mechanics Series, https://doi.org/10.13052/rp-9788743814139

in inaccessible areas [8],[9],[16]. GPR complements these techniques by mapping subsurface conditions, revealing soil instability or voids that affect foundation behavior [10]. Recent advances include digital twins; virtual models integrating real-time data to simulate and predict structural responses to hazards or interventions [11]. Combined with IoT technologies, these models enable adaptive and predictive conservation strategies. In summary, SHM has become essential for sustainable heritage management, bridging knowledge gaps and guiding preservation decisions. For monuments like Temple II, it ensures both structural stability and the enduring transmission of cultural and historical value.




**Fig. 1** Left: Geographical location of Tikal National Park, WorldAtlas.com (red squared). Upper-right: The Temple of the Masks (Temple II), evaluated in this research. Downright: Temple of the Great Jaguar (Temple I)

## On-Site Assessment Methodology

### *Ambient vibration tests*

A series of ambient vibration tests were conducted at the temple to determine their dynamic modal properties. Nine portable-wireless sensors [14] were used for these tests. The testing program consisted of three measurement setups. The layouts of the sensors are illustrated in Figure 2. For all configurations, five out of nine sensors were considered as reference: four at level 3 and one at the ground level. The remaining four sensors were placed at level 2 for setup 1, at level 1 for setup 2 and level 4 for setup 3 as rovers. The duration for all setups was 20 minutes at a 128 Hz sample rate.

### *Sclerometric tests*

Schmidt hammer tests were performed at 64 points on the pyramid to establish a characteristic value for the material's compressive strength. The method provides a non-destructive estimation of compressive strength by measuring the rebound number, which correlates with material hardness and strength. The relationship between the rebound number and compressive strength is established empirically and can be expressed as $f_c = a \cdot R^b$, where $f_c$ is the compressive strength, R is the rebound number, and $a$ and $b$ are material-specific constants.

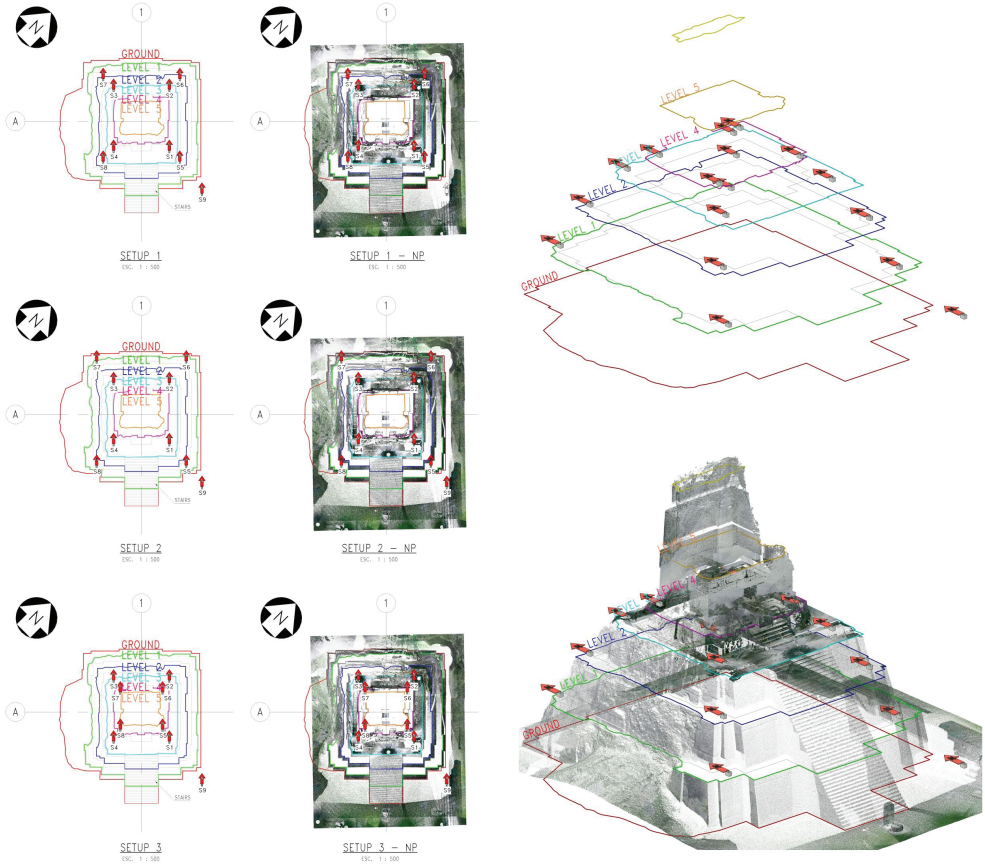


**Fig. 2** Setup 1 to 3. Ambient vibration test setup (velocity)

## *3D Geometric Survey*

A laser scanning survey was conducted around the pyramid to produce a high-resolution 3D point-cloud model. Thirty-one scan positions captured up to 360,000 points per second, accurately recording the structure's geometry and external features (Figure 3). The processed data provided a precise 3D reference for structural and geometric analysis, including assessments

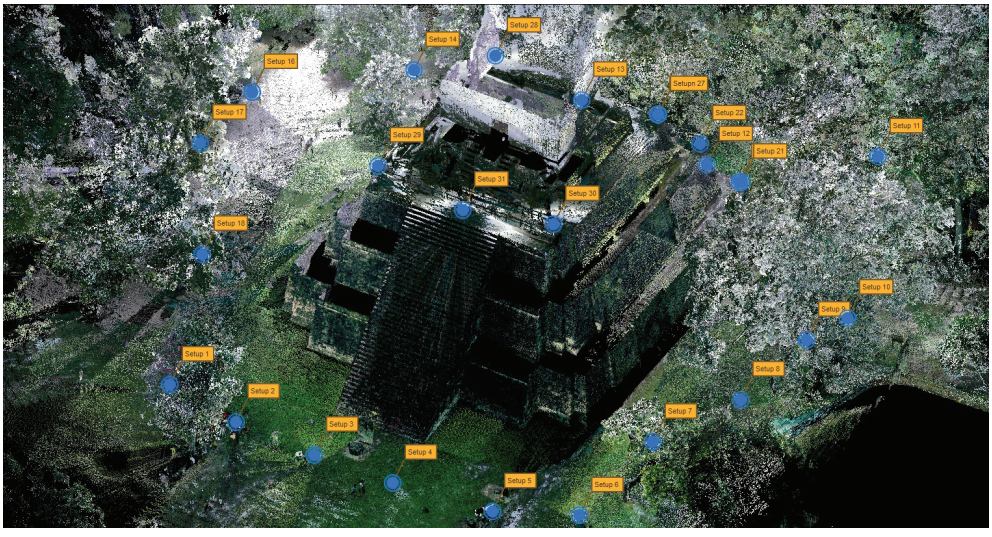

**Fig. 3** Laser Scanner Positions during survey

of verticality and differential settlements. These measurements revealed potential tilting and foundation movements, offering key insights into the pyramid's current condition and long-term stability.

## Results and Discussion

### *Dynamic properties*

Well-established techniques were employed in both the frequency and time domains to obtain the dynamic parameters of the temple. The Enhanced Frequency Domain Decomposition (EFDD) was used for the frequency domain. For the time domain analysis, the Stochastic Subspace Identification (SSI) approaches—Unweighted Principal Components (UPC) and Canonical Variate Analysis (CVA)—were applied. All the analyses were developed using the ARTeMIS Modal software [15]. The results obtained from these analyses are presented below.

**Table 1** Frequencies ($f$) and damping ratios ($\beta$). Ambient vibration tests (setup 1-2-3).

| N° | Freq. [Hz] EFDD | Freq. [Hz] SSI-UPC | Freq. [Hz] SSI-CVA | **Freq. [Hz] Avg.** | $\beta$ [%] EFDD | $\beta$ [%] SSI-UPC | $\beta$ [%] SSI-CVA | **$\beta$ [%] Avg.** | **Predominant Direction Modal Shape** |
|---|---|---|---|---|---|---|---|---|---|
| 1 | 4.07 | 4.08 | 4.07 | **4.07** | 0.5 | 1.6 | 1.0 | **1.0** | Bending (X) |
| 2 | 4.24 | 4.26 | 4.24 | **4.25** | 1.2 | 2.2 | 1.8 | **1.7** | Bending (Z) |
| 3 | 8.01 | 8.05 | 8.08 | **8.05** | 2.4 | 2.2 | 2.8 | **2.5** | Vertical (Y) |

### *Sclerometric tests*

García de Miguel et al. [12] describe the nearby Great Jaguar Pyramid as composed of ashlar masonry walls filled with *embono*—a lime mortar with limestone fragments—forming a dense, low-void structure. The fine, porous limestone is prone

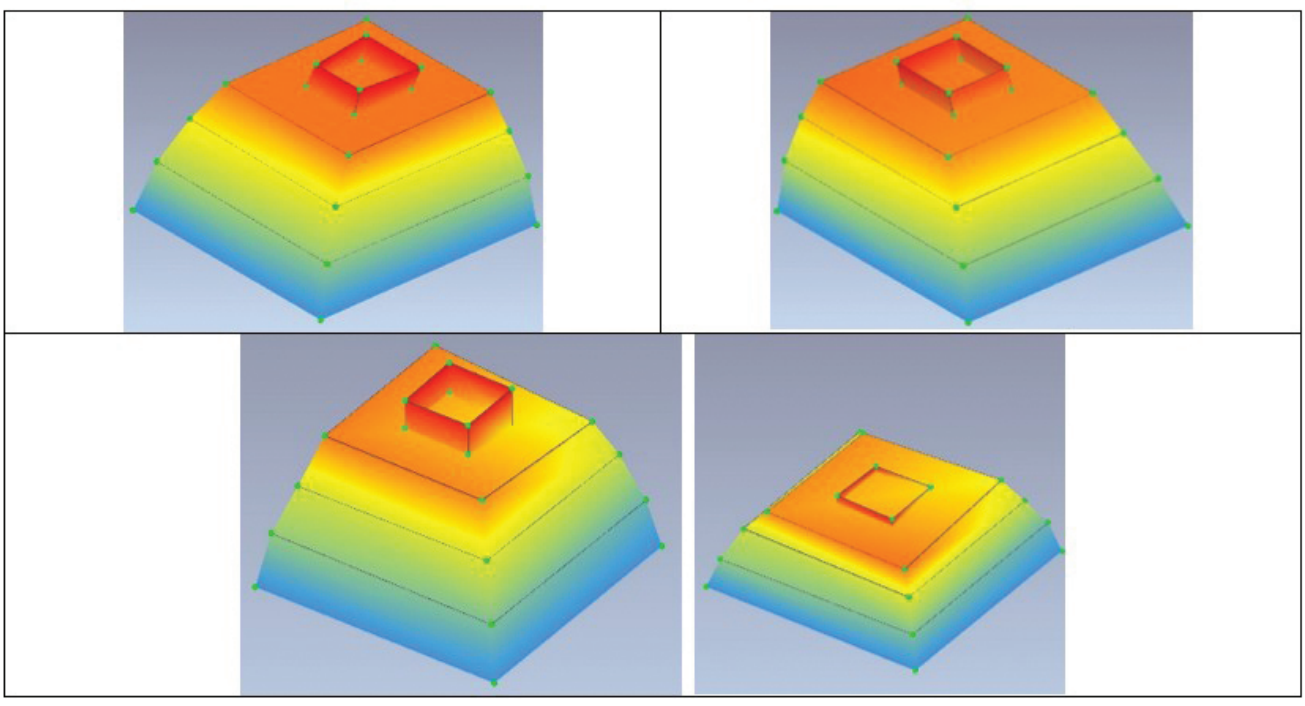

**Fig. 4** Modal Shapes. Upper-left: f=4.07[Hz], upper-right: f=4.25[Hz], down f=8.05[Hz]. ARTeMIS Modal Software [15]

to erosion and biological growth. As Temple II shares similar materials and techniques, these findings likely apply to it as well, suggesting comparable deterioration mechanisms such as loss of *embono* cohesion and limestone decay, which offer key insights for its preservation.

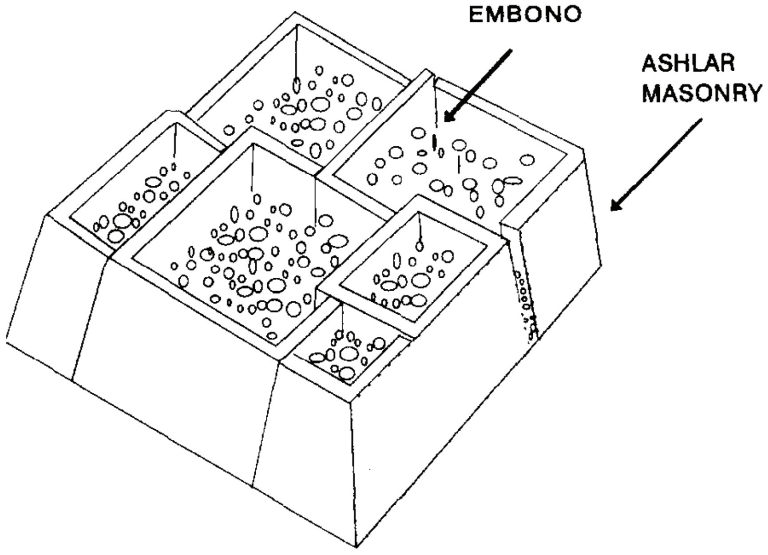


**Fig. 5** The schematic material structure of the Temple [12]

According to M. Kržan et al. [13], the compressive strength of ashlar masonry depends on morphology and construction quality, averaging 6.05 MPa and typically ranging from 4 to 8 MPa. The Schmidt hammer tests on Temple II yielded a characteristic value of 5.97 MPa, showing an acceptable correlation with the previously cited study. As shown in Figure 6, values range from 3.7 to 8.3 MPa, reflecting the high heterogeneity also reported in their work and confirming the correlation between rebound number and compressive strength. The characteristic compressive strength was obtained using a Kernel Density Estimation (KDE) method, which identifies the most probable value within the empirical distribution of test results. Following the configuration described by García de Miguel et al. [12], a significant portion of the structure consists of embono, a lime mortar with limestone fragments forming a dense, low-void matrix. Under the BS EN 459-1 [17] classification,

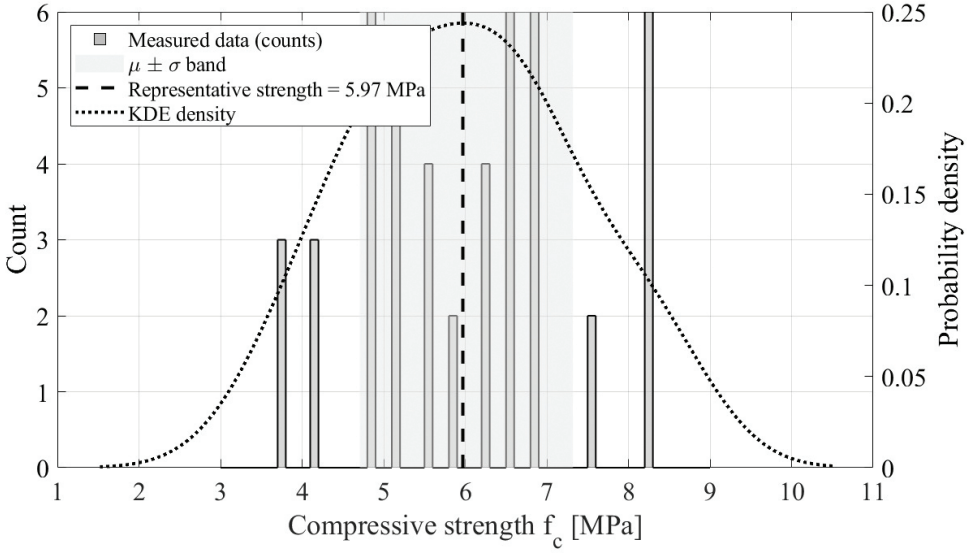


**Fig. 6** Estimation of compressive strength for ashlar masonry using KDE method

this material can be conservatively considered as an NHL 2 lime mortar ($f'_n$ = 2 MPa). Since most of the pyramid is composed of embono while the mechanical characterization was performed only on the ashlar masonry, an equivalent structural compressive strength was estimated assuming a contribution of 30 % from the ashlar masonry and 70 % from the embono. Based on the characteristic values reported, the pyramid's overall characteristic compressive strength was therefore taken as 3.2 MPa, for use in material characterization and subsequent numerical modeling.

## *Geometry survey*

The laser scanning survey produced a detailed 3D dataset that enabled a comprehensive analysis of the pyramid's geometry and structural behaviour. The resulting point cloud accurately captured its dimensions and allowed assessment of external contours, vertical alignment, and overall stability. The analysis revealed differential settlements (rocking) across structural blocks, decreasing from base to top: 278 mm at the first block, 169 mm between levels 1–2, and 68 mm between levels 2–3. These settlements are critical for structural evaluation, while no differential movement was observed in the opposite direction.

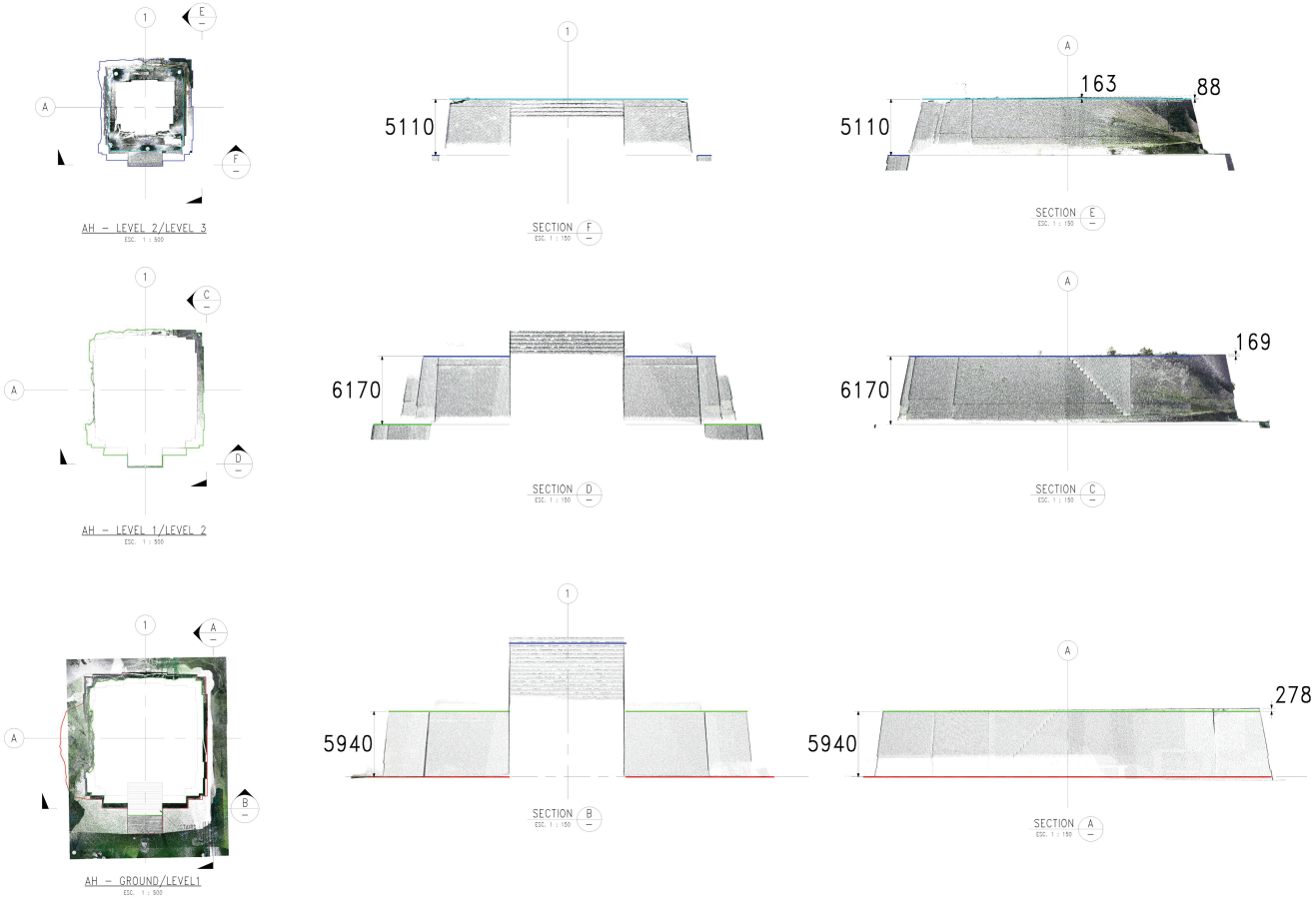


**Fig. 7** Estimated rocking between pyramid blocks using 3D laser scanning. Up: upper block, between level 3 and 2. Middle: middle block, between level 2 and 1. Down: ground block, between level 1 and ground

## *Calibrated model*

A key step after structural assessment and SHM analysis is calibrating a mathematical model to evaluate the structure's condition and simulate its response to earthquakes, soil effects, extreme weather, or long-term degradation. To develop such a model, it was essential to obtain on-site data: the geometry provided a volumetric measure of the structure, the sclerometric tests allowed the derivation of mechanical properties, and the vibration measurements enabled model calibration for subsequent scenario simulations. Regarding the characteristic values of mechanical strength, Table 2 summarizes those considered for the model.

**Table 2** Calibrated mechanical properties for simplified model

| N° | Variable | Symbol | Value | Unit | Comments |
|---|---|---|---|---|---|
| 1 | Density | $\gamma$ | 2200 | $kg/m^3$ | Calibrated based on clay soils improved with lime or cement: 1700-2200 $kg/m^3$ |
| 2 | Compressive Strength | $f_c^{'}$ | 3.2 | $MPa$ | Average value from the sclerometric test |
| 3 | Young's Modulus | $E$ | 480 | $MPa$ | $E = 150 f_c^{'}$ |
| 4 | Poisson Ratio | $\nu$ | 0.15 | $MPa$ | Calibrated based on clay soils improved with lime or cement: 0.15 – 0.35 |
| 5 | Shear Modulus | $G_c$ | 209 | $MPa$ | $G_c = E/2(1+\nu)$ |

The density in Table 2 follows M. Kržan & V. Bosiljkov (2023) [13], while compressive strength was obtained considering a weighting of 30 % for the characteristic compressive strength of the ashlar masonry (5.97 MPa) and 70 % for the *embono* material (2 MPa), a uniform characteristic compressive strength of 3.2 MPa was assumed for the pyramid. The remaining parameters were estimated from empirical and reference data to define the model's stiffness. Based on these parameters, a finite element model was developed in Ansys software. The model was built from the point cloud obtained through laser scanning, which was cleaned and processed to generate a geometry suitable for meshing. A solid mesh was created with approximately 94,000 quadratic elements, using finer discretization in areas with sharp angles or geometric details requiring higher resolution, shown in Figure 8:

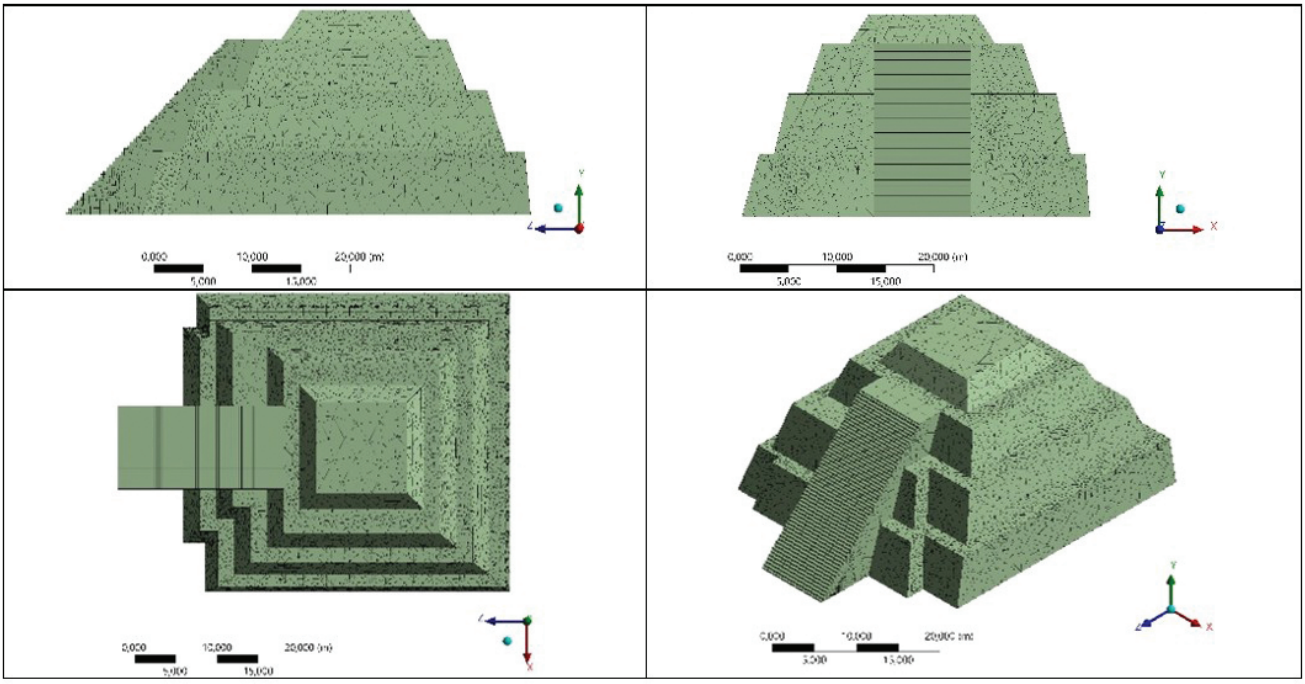

**Fig. 8** Different views for the FE model developed in Ansys

The model included only self-weight loading to estimate the natural frequencies and mode shapes. Thirty modes were initially computed to assess the cumulative effective modal mass. The main modal shapes and their corresponding frequencies are presented below.

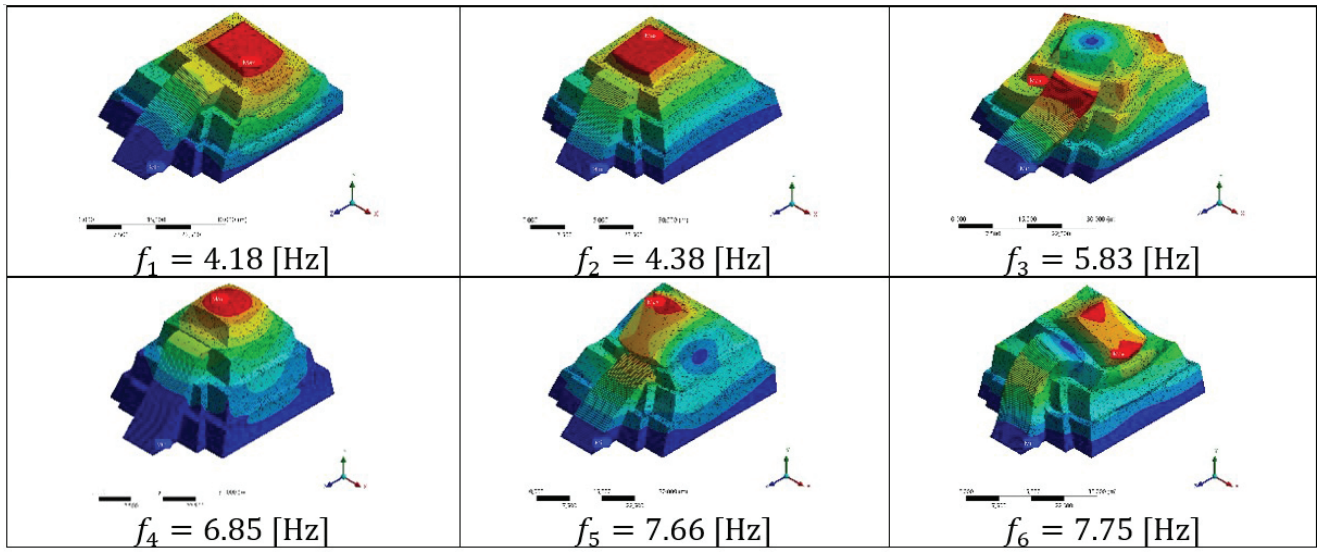


**Fig. 9** Modal frequencies and shapes for the FE model

**Table 3** Modal frequencies and modal mass percentage for each mode. FE model

| Mode | Modal Freq. [Hz] Model | Predominant direction | % Modal Mass X | % Modal Mass Z | % Modal Mass Y (vert.) |
|---|---|---|---|---|---|
| 1 | 4.18 | Bending | 55.60 | 0.07 | - |
| 2 | 4.38 | Bending | 0.08 | 57.20 | 0.02 |
| 3 | 5.83 | Torsional | 0.15 | - | - |
| 4 | 6.85 | Vertical | - | - | 52.26 |
| 5 | 7.66 | Bending | 0.01 | 13.82 | 0.06 |
| 6 | 7.75 | Bending | 17.23 | - | - |

Finally, Table 4 presents a comparison between the natural frequencies obtained from ambient vibration testing and those derived from the finite element model, which was developed based on the field survey data. From the table, it can be observed that the frequencies predicted by the model are in reasonable agreement with those identified from ambient vibration measurements, confirming that the calibrated numerical model provides an acceptable representation of the structure's dynamic behavior.

**Table 4** Frequency comparison. Ambient vibration results and FE model

| Mode | Modal Freq. [Hz] Ambient Vibration | Modal Freq. [Hz] FE Model | Difference [%] | Predominant direction |
|---|---|---|---|---|
| 1 | 4.07 | 4.18 | 2.7 | Bending |
| 2 | 4.25 | 4.38 | 3.1 | Bending |
| 3 | 8.05 | 6.85 | 14.9 | Torsional |

## Conclusions

This study presents a structural assessment of Temple II, focusing on its dynamic behaviour, geometry, and material properties. Ambient vibration testing identified modal frequencies, damping ratios, and mode shapes, while 3D laser scanning

detected differential settlements and deviations from verticality. The analysis revealed up to 278 mm of settlement (tilt ≈ 0.43°) along one principal direction. Schmidt Hammer tests showed variable compressive strength (5.97 MPa characteristic value), consistent with Kržan [13] and confirming the reliability of this non-destructive method. A FE model, calibrated with field data, provided a reasonable representation of the temple's dynamic response. The findings indicate potential risks related to settlement and emphasize the need for long-term monitoring and improved material characterization. Further soil–structure interaction evaluation is recommended for a better understanding of its role in the observed deformation and stability. This work demonstrates the value of an integrated SHM approach—combining vibration testing, geometric surveys, and non-destructive material evaluation—to assess structural integrity while minimizing intervention. Continuous monitoring enables early detection of deterioration and supports preventive conservation. Future efforts should include permanent sensor systems, refined soil–structure studies, and advanced digital modelling (e.g., digital twins and parametric simulations). Extending this methodology to nearby temples and simulating extreme events such as earthquakes or severe weather will improve predictive analysis and support long-term preservation of Tikal's heritage.

## References


1. M. Sangirardi, A. Amorosi, G. de Felice (2020). A coupled structural and geotechnical assessment of the effects of a landslide on an ancient monastery in Central Italy, Engineering Structures, Volume 225, 111249, ISSN 0141-0296, https://doi.org/10.1016/j.engstruct.2020.111249.
2. R. Aguilar, M. Pando, C. Briceño, G. Zavala, B. Castañeda, R. Perucchio, S. Uceda (2018). Structural and geotechnical engineering assessment of Huaca de la Luna – A massive earthen Moche culture pyramid in Northern Peru, Journal of Cultural Heritage, Volume 34, Pages 83-94, ISSN 1296-2074, https://doi.org/10.1016/j.culher.2018.04.006.
3. M. Rossi and D. Bournas (2021). Structural Health Monitoring and Management of Cultural Heritage Structures: A State-of-the-Art Review. Journal of Civil Engineering and Management, 27(3), 134–148. https://doi.org/10.3846/jcem.2021.14202
4. Coe, W. R. (1986), Tikal: A Handbook of the Ancient Maya Ruins. University of Pennsylvania Museum.
5. I. Šprajc (2016). Astronomical Alignments in Ancient Maya Architecture. Latin American Antiquity, 27(2), 143-160.
6. S. Mazzetto (2024). Integrating Emerging Technologies with Digital Twins for Heritage Building Conservation: An Interdisciplinary Approach with Expert Insights and Bibliometric Analysis. Heritage, 7(11), 6432-6479. https://doi.org/10.3390/heritage71103002
7. P. Clemente (2018). Extending the Life-Span of Cultural Heritage Structures". Journal of Civil Structural Health Monitoring. 8:171–179. https://doi.org/10.1007/s13349-018-0278-3(0123456789().,-volV)(0123456789().,-volV)
8. N. Xu, D. Huang, S. Song, X. Ling, C. Strasbaugh, A. Yilmaz, R. Qin, R. (2021). A volumetric change detection framework using UAV oblique photogrammetry – a case study of ultra-high-resolution monitoring of progressive building collapse. International Journal of Digital Earth, 14(11), 1705–1720. https://doi.org/10.1080/17538947.2021.1966527
9. Y. H. Jo & S. Hong (2019). Three-Dimensional Digital Documentation of Cultural Heritage Site Based on the Convergence of Terrestrial Laser Scanning and Unmanned Aerial Vehicle Photogrammetry. ISPRS International Journal of Geo-Information, 8(2), 53. https://doi.org/10.3390/ijgi8020053
10. A. Kanli, G. Taller, P. Nagy, P. Tildy, Z. Pronay, E. Toros (2015). GPR survey for reinforcement of historical heritage construction at fire tower of Sopron, Journal of Applied Geophysics, Volume 112, Pages 79-90, ISSN 0926-9851, https://doi.org/10.1016/j.jappgeo.2014.11.005.
11. A. Darwish & A.E. Hassanien (2022). IoHCT: Internet of Cultural Heritage Things Digital Twins for Conservation and Health Monitoring of Cultural in the Age of Digital Transformation. In Digital Twins for Digital Transformation: Innovation in Industry (pp. 1–21). Springer. https://doi.org/10.1007/978-3-030-96802-1_1
12. J.M. Garcia De Miguel, L. Sanchez-Castillo, J.J. Ortega-Calvo, J.A. Gil, C. Saiz-Jimenez (1995), Deterioration of building materials from the Great Jaguar Pyramid at Tikal, Guatemala, Building and Environment, Volume 30, Issue 4, Pages 591-598, ISSN 0360-1323, https://doi.org/10.1016/0360-1323(94)00055-W.
13. M. Kržan & V. Bosiljkov. (2023) Compression and In-plane Seismic Behaviour of Ashlar Three-leaf Stone Masonry Walls. International Journal of Architectural Heritage 17:6, pages 829-845.
14. Micromed (2012) Tromino: Portable ultra-light acquisition system for seismic noise and vibration- User's manual. Macromed, Italy.
15. Structural Vibration Solutions (2016) ARTeMIS modal software. Version 6. SVS, Denmark.
16. Canuto, M. A., Estrada-Belli, F., Garrison, T. G., Houston, S. D., Acuña, M. J., Kováč, M., Marken, D., Nondédéo, P., Auld-Thomas, L., Castanet, C., Chatelain, D., Chiriboga, C. R., Drápela, T., Lieskovský, T., Tokovinine, A., Velasquez, A., Fernández-Díaz, J. C., & Shrestha, R. (2018). Ancient lowland Maya complexity as revealed by airborne laser scanning of northern Guatemala. Science, 361(6409), eaau0137. https://doi.org/10.1126/science.aau0137csu-sdsu.primo.exlibrisgroup.com+8datadryad.org+8hal.science+8
17. BSI Standards Publication. (2015). BS EN 459-1:2015, Building lime—Part 1: Definitions, specifications and conformity criteria. BSI.